# Improving thermal insulation of timber frame walls by retrofitting with vacuum insulation panels – experimental and theoretical investigations

Sveipe, E., Jelle, B. P., Wegger, E., Uvsløkk, S., Grynning, S., Thue, J. V., Time, B., Gustavsen, A.

Citation for the published version (APA 6th)
Sveipe, E., Jelle, B. P., Wegger, E., Uvsløkk, S., Grynning, S., Thue, J. V., Time, B., Gustavsen, A. (2011). Improving thermal insulation of timber frame walls by retrofitting with vacuum insulation panels – experimental and theoretical investigations. *Journal of Building Physics, 35*(2), 168-188. doi:10.1177/1744259111403439

# Improving Thermal Insulation of Timber Frame Walls by Retrofitting with Vacuum Insulation Panels – Experimental and Theoretical Investigations

Erland Sveipe [a], Bjørn Petter Jelle [ab]*, Erlend Wegger [a], Sivert Uvsløkk [b]
Steinar Grynning [b], Jan Vincent Thue [a], Berit Time [b], Arild Gustavsen [c]

[a] Department of Civil and Transport Engineering, Norwegian University of Science and Technology (NTNU), NO-7491 Trondheim, Norway.
[b] Department of Materials and Structures, SINTEF Building and Infrastructure, NO-7465 Trondheim, Norway.
[c] Department of Architectural Design, History and Technology, Norwegian University of Science and Technology (NTNU), NO-7491 Trondheim, Norway.

* Corresponding author: bjorn.petter.jelle@sintef.no (e-mail), 47-73-593377 (phone), 47-73-593380 (fax).

## ABSTRACT

Many of the Norwegian buildings from the 1960s-1980s with timber frame walls are ready for retrofitting. Retrofitting of these buildings with vacuum insulation panels (VIPs) may be performed without significant changes to the buildings, e.g. extension of the roof protruding and fitting of windows. Effectively, U-values low enough to fulfil passive house or zero energy requirements may be achieved, thus contributing to a reduction of the energy use and $CO_2$ emissions within the building sector. Retrofitting with VIPs on the exterior side is normally considered as a better solution; however, it may cause condensation in the wall. To investigate this and the interior option, four different wall fields were tested. One of them was a reference wall field built according to Norwegian building regulations from the 1970s, and three other fields represent different ways of increasing the thermal insulation level. In addition to the experiments, numerical simulations were performed where temperature, relative humidity (RH), and surface wetness were measured. In total, the results from the experiments, simulations, and condensation controls conclude that timber frame buildings insulated with 100 mm mineral wool, might be retrofitted at the outside by adding 30 mm VIPs. However, this method for retrofitting provides limits to outdoor temperature, indoor moisture excess and indoor temperature.

**Keywords:** Thermal insulation, Retrofitting, Timber frame wall, Vacuum insulation panel, VIP.

## 1 INTRODUCTION

An U-value of 0.35 W/($m^2$K) (about 10 cm mineral wool) in walls was required in Norwegian buildings in the 1970s (Building regulations of 1969), whereas today the requirement is an U-value of 0.18 W/($m^2$K) (TEK 1997), i.e. nearly 50 % less. The passive houses have even higher requirements. Furthermore, $CO_2$ emissions from the building stock is an issue. To reduce $CO_2$ emissions by thermal insulation (McKinsey 2009), vacuum insulation panels (VIPs) are suitable as their environmental loading is similar to conventional insulation materials (Binz et al. 2005). The VIP is built up of a fumed silica core enclosed by a high barrier envelope to maintain the vacuum. More information on the VIP construction may be found in Willems et al. (2005) or Tenpierik (2009). The ageing of VIPs is mainly caused by reduction of vacuum over time, see Baetens et al. (2010) and Wegger et al. (2010). A major challenge using VIPs is the risk of puncturing. A punctured panel has about 5 times higher thermal conductivity than an intact one, i.e. a conductivity of about 0.02 W/(mK) for a punctured VIP (Binz et al. 2005). In general, the use of VIPs requires a design of the structure and high level of precision and use of a secure workmanship because the VIPs cannot be adjusted or cut at the construction site.

Retrofitting of buildings with VIPs is advantageous because passive house standards may be achieved without major changes to the building structure. Adding insulation on the exterior prevents moisture problems as the temperature in the old wall structure rises, and furthermore reduces the effect of thermal bridges. However, a vapour tight layer on the cold side increases the risk of condensation inside the wall. SINTEF Building Research Design Guides (SINTEF 523.002, 2008) requires that ¾ of the total amount of insulation must be located on the cold side of the vapour barrier. Yet, if thermal resistance of VIPs is reduced because of ageing or puncture there is a risk of condensation. This work investigates both ways of retrofitting walls, one with VIPs on the cold side and one with VIPs on the warm side. Test wall fields were placed between two climate chambers with indoor and outdoor climate, respectively. Moisture and temperature conditions in the wall were logged, analysed and compared with the numerical simulations. This method for retrofitting with VIPs discusses and provides limits to outdoor temperature (climate zones), indoor moisture excess (humidity classes), and indoor temperature (building type).

# 2 EXPERIMENTAL

## 2.1 Description of Test Module and Fields

The test module contains four fields as seen in Figs.1-3. Field 3 (F3) is built without VIPs and represents the original structure before retrofitting, i.e. a reference field of a timber frame wall from the 1970s. The three other fields (F1, F2 and F4) represent three different ways of improving the thermal insulation of the reference field (Fig.2).

- **F1:** Outside 30 mm VIP
- **F2:** Outside 20 mm VIP
- **F3:** Reference field
- **F4:** Inside 30 mm VIP

The four fields are separated by plastic film and extruded polystyrene (XPS), i.e. separated with respect to moisture and heat transport. Fig.1 illustrates the test module with the four fields in 3D, whereas Fig.2 shows a horizontal cross-section of the test module.

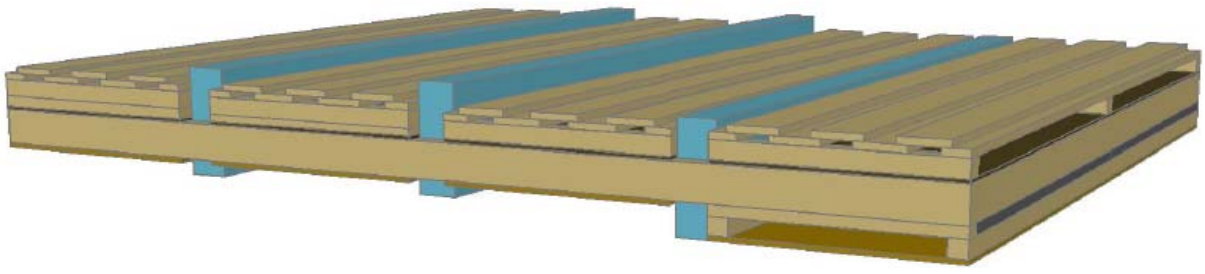

**Figure 1. The test module in 3D view, as seen from the bottom.**

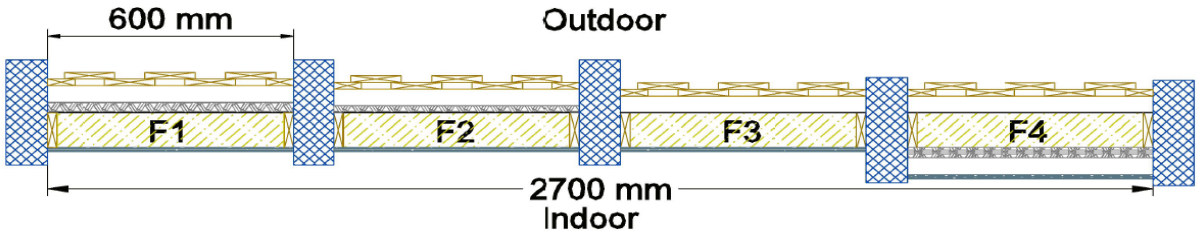


**Figure 2. Horizontal cross-section of the test module. Note that the fields have no vapour barrier.**

The build-up of Field 2 from outdoor to indoor (Fig.2 and Fig.3).

- Vertical wooden cladding
- Furring strip (attached with a tailor-made fastening bracket, shown in ch. 2.2)
- VIPs, joint not taped (attached with the same tailor-made fastening bracket)
- Wind barrier (bitumen-impregnated paper, in common use in the 1970s)
- Mineral wool
- Plasterboard

Normally, the wall should have a vapour barrier as well, but this was omitted due to a relative short timeframe for the experiment. Not installing a vapour barrier represents a conservative modification and might be considered as a worst-case scenario.

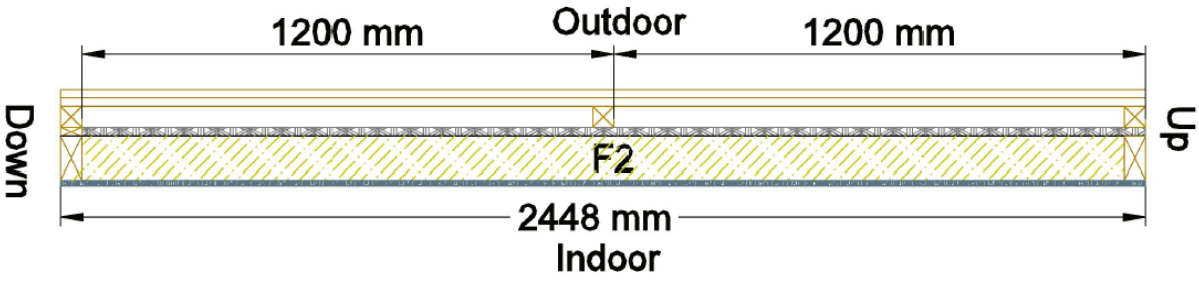


**Figure 3. Vertical cross-section of Field 2. Note that the field has no vapour barrier, only the vapour tight VIPs at the exterior side (F2 from Fig.2).**

The VIPs used in this work are of the type Vacupor NT - B2 from the producer Porextherm. Vacupor NT – B2 is a micro porous insulation material and consists of inorganic oxides. The main constituent is fumed silica. The other components are opacifiers for minimizing infrared radiation, and silicates. The panels are heat sealed with a high barrier film to maintain the vacuum (Porextherm 2009).

## 2.2 VIP Fastening Bracket

In order to minimize the thermal bridges and being able to fasten the VIPs in an effective way, tailor-made fastening brackets were made (Fig.4 and Fig.5). The new VIP fastening brackets were made of a steel plate that is cut and bent so it can be fixed to the behind laying stud and at the same time hold the furring strip where the wooden cladding are fastened. This way the joints between the VIPs will be reduced to a minimum, i.e. the thickness of the steel plate. Figure 4 illustrates a 3D model of one of the main resulting fastening brackets.

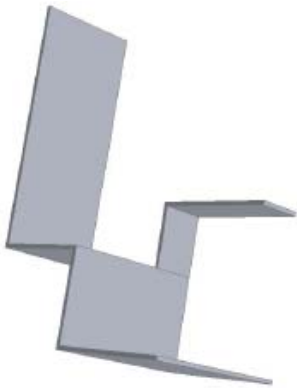

**Figure 4. A 3D model of one of the main VIP fastening brackets.**

Figure 5 shows the application of the VIP fastening brackets in practise, where different steps during the implementation of the brackets are shown. Note that the fastening brackets were

taped around before installation in order to reduce the probability of VIP puncture due to sharp edges in the brackets.

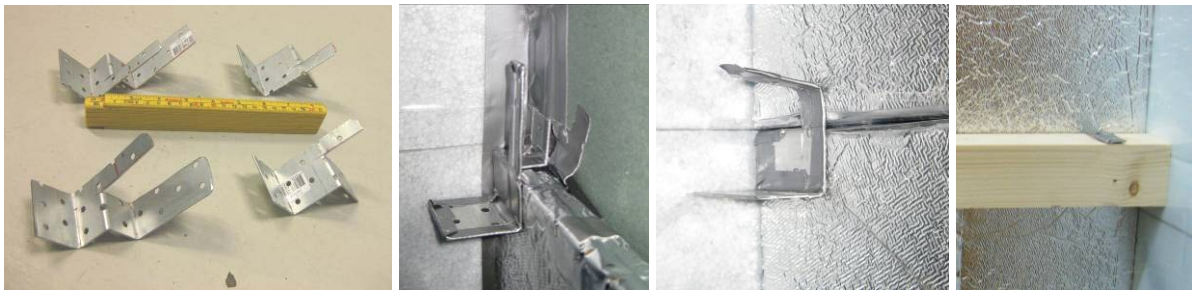

**Figure 5. Principle of the fastening bracket. The left photo shows the fastening brackets used in the middle of the wall (between two VIPs, fastened on a wooden stud), and fastening brackets used at the top plate. The three other photos show different stages in the installation of the fastening bracket between two VIPs.**

A fastening bracket made of steel makes a thermal bridge in the structure. Other materials with lower thermal conductivities may be used for the fastening brackets, e.g. stainless steel, where one requirement is sufficient high mechanical strength, naturally. The size of the thermal transmittances applying various fastening brackets was addressed and compared to a traditional way of fastening VIPs, which was simulated in the two-dimensional finite element program THERM (2003), and where the linear thermal transmittance of each thermal bridge version was calculated according to EN ISO 10211 (2007). The resulting average linear thermal transmittance of the horizontal joint between two VIPs is a result of the fastening bracket thermal transmittance (only present over the wooden stud) and the thermal transmittance of the horizontal joint between two VIPs. Their influence is determined according to a ratio of their length and the total length. In this context, the details of these calculations, both method and results, are not shown in order to not make this article too extensive.

The results show that even if the thermal transmittance of the fastening bracket is larger than the thermal transmittance of the furring strip, the average thermal transmittance per metre of VIP joint is smaller for the fastening bracket. The average linear thermal transmittance of the fastening bracket used in the laboratory experiments (tape-enveloped steel) has been calculated to 0.0083 W/(mK), which is 69 % lower and thus better than the traditional furring strip fastening method with a calculated average linear thermal transmittance of 0.027 W/(mK). Applying tape-enveloped stainless steel (instead of carbon steel) reduces the average linear thermal transmittance further to 0.0067 W/(mK).

## 2.3 Surface Wetness Sensor

In order to be able to measure condensation on a surface a tailor-made moisture sensor was developed (Fig.6). An air humidity sensor may show a relative humidity (RH) below 100 %, while condensation has actually occurred on the adjacent cold surface. The principle is to measure the electrical resistance on a thin material taped on the respective surface, i.e. the measurement will be as close to the material surface as possible. Different materials for use in the moisture sensor were considered and tested. Finally, the choice was a regular copy paper (Lyreco Budget, 80 g/m$^2$). The sensor consists of double-sided tape, plastic-insulated single-wired 1.5 mm$^2$ cables, and a sheet of copy paper. The moisture sensor is henceforth called the *wetness sensor*, and is depicted in Fig.6.

The electrical resistance of the wetness sensor was measured with a wood moisture content meter, i.e. the electrical resistance was expressed by the moisture content in spruce (at 20°C).

The sensor was calibrated in advance by measuring the moisture content values for different RH in a climate chamber at 10°C. The result of this calibration made it possible to convert the measured moisture content from the experiment to RH values by a linear function on the form y = ax + b, where the ”a” and ”b” values were calculated. The moisture content measured when condensation occurred on the sensor was also noted. Note that several errors related to this method is not discussed in this context. Hence, the wetness sensor is to be considered as an indicator of RH and condensation.

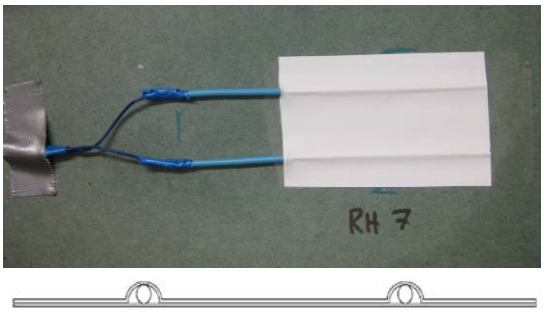


**Figure 6. The wetness sensor consists of double-sided tape, single-wired cable and a paper sheet.**

The tailor-made wetness sensor proved to be quite trustworthy during the laboratory test. Even though the sensor originally was made as an indicator for condensation, the sensor proved also to be relatively reliable for RH values between 70 – 100 %. The wetness sensor and the RH air sensor were in good agreement when placed at the same location. The values below 100 % are equivalent with RH while the values above 100 % indicate condensation. Note that the wetness sensor did not measure lower RH values than about 60 % because the electrical resistance was then too high for the wood moisture content meter to measure. However, as noted above, the wetness sensor is primarily an indicator of RH and condensation, i.e. the reliability, e.g. versus several repetitive condensation cycles, should then be further tested.

## 2.4 Temperature and Moisture Measurements

Altogether, 36 sensors of three different types were used in experiment, i.e. thermocouples (T), air humidity sensors including thermocouples (RH) and wetness sensors (C) as depicted in Fig.7. The thermocouples are familiar and consist of a cable with two separate conductors, i.e. copper and constantan. The cables are twined and soldered together at the tip where the measurements based on varying electrical potentials take place. The air humidity sensors were of the type Vaisala humidity and temperature transmitter Type HMP233, abbreviated as RH air sensors.

The most critical location for condensation was considered to be on the warm side of the VIPs in Field 1 and Field 2 (Fig.7), and at the warm side of the wind barrier (WB) at the reference field (F3). The thermal resistance of the wind barrier is marginal and the type of wind barrier used has a small water vapour resistance, i.e. condensation was expected to occur on the wind barrier as well as on the VIP surface. Hence, for practical reasons and the desire of having the sensors at the same locations for all four fields, most of the sensors were located at the warm side of the wind barrier. The sensors at the top and the bottom were located 100 mm from the sills where the natural convection in the mineral wool was considered to have the largest influence. The sensors at the middle were located directly within the joints of the VIPs, i.e. 1200 mm above the bottom sill. Furthermore, there were also sensors at other locations in the wall module. A wetness sensor were glued directly over the horizontal joint between two VIPs in F1 and F2 as shown in Fig.7, i.e. F1 and F2 had wetness sensors on both sides of the

wind barrier in the middle of the field. There were also thermocouples in all four ventilated air cavities as depicted in Fig.7. In addition, air temperature and RH were measured in both climate rooms.

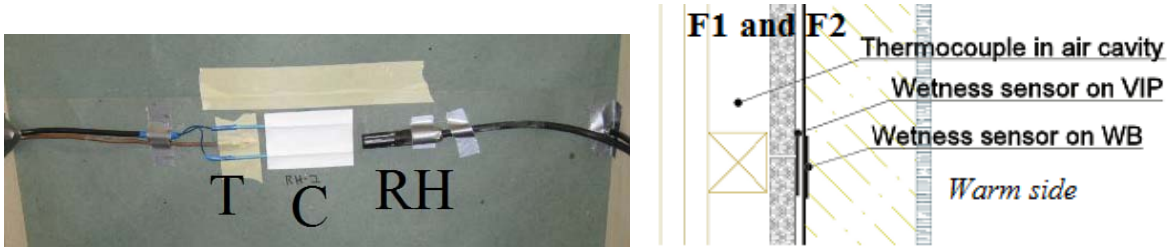


**Figure 7. Left photo depicts the thermocouple (T), wetness sensor (C), and RH air sensor (RH) as installed on the wind barrier before the mineral wool was added. Right drawing shows a cross-section of F1 and F2 with a wetness sensor both on the wind barrier and on the joint between two VIPs at the middle of the fields. The thermocouple in the air cavity is also shown, while other sensors on the wind barrier (WB) are not depicted.**

The 36 sensors gave a total amount of 42 logging channels due to six combined humidity and temperature sensors (RH air sensors). Three different logging systems were used in the experiment. Due to the large number of sensors, the thermocouples and the air humidity sensors were logged by two systems, i.e. Solartron 35951C I.M.P. connected to Orchestrator 1.4.7 software, and FLUKE Hydra data logger 2625A with appurtenant software. The wetness sensors required a separate logging system, i.e. a logger made by SINTEF containing a Greisinger GMH 830 material moisture meter, which was computer interfaced via LabVIEW8.6 software.

## 2.5 Test Procedure

The test wall module was built between two climate rooms in the laboratory. The temperature at the cold side was intended to be -20°C, but due to climate room regulation limitations the outdoor temperature was adjusted to -18°C. The relative humidity in the outdoor climate was not controlled, but was in the order of RH ~ 60 %. In the indoor climate the temperature was held constant at 20°C, while the RH was adjusted in the following steps of 10 %:

1. RH 30 % (~ 4 g/m$^3$)*
2. RH 40 % (~ 6 g/m$^3$)*
3. RH 50 % (~ 8 g/m$^3$)*
4. RH 60 % (~ 10 g/m$^3$)*

*approximately the internal moisture excess that equals the given indoor RH for a indoor temperature of 20°C, an outdoor RH of 60 %, and an outdoor temperature of -18°C.

These moisture levels are henceforth called *climate steps*. The term internal moisture excess represents the difference in moisture content (g/m$^3$) from the indoor to the outdoor air (EN ISO 13788, 2001). To calculate the value the indoor and outdoor air temperature, RH outside, moisture production inside and ventilation degree are taken into account. The term is useful in practical condensation calculations and divides different building types into humidity classes (EN ISO 13788, 2001).

## 2.6 Numerical Simulations of Temperature and Moisture Performance

Both 1D and 2D simulations of thermal and hygrothermal performance of the fields have been performed. The two simulation programs WUFI Pro (WUFI 1D 2010) and WUFI 2D (WUFI 2D 2010) have been used. The 1D calculations only simulate the gross structure of the fields, i.e. the thermal and hygrothermal performance in the centre of a VIP. The 2D simulations also

account for possible heat and vapour transport trough the joint between two VIPs. The climate file applied in the simulations is based on the logged temperature and RH in the climate rooms during the experiment. That is, the simulation results and the logged values from the experiment could be compared directly. The material data applied in the simulations was partly from WUFI, partly from EN ISO 10456 (2007) and from some other literature sources. In the simulations, the VIPs were treated as two separate materials in three layers, i.e. VIP envelope, VIP core and again VIP envelope, where the thickness of the VIP envelope was set to 1 mm to avoid problems in the numerical solver. As a result of this, and based on a 0.1 mm thick VIP envelope thermal conductivity of 0.54 W/(mK) (Tenpierik and Cauberg 2007), the adjusted thermal conductivity of the VIP envelope used in the simulations was 5.4 W/(mK) for heat flow perpendicular to the envelope, and 0.054 W/(mK) for heat flow longitudinal to the envelope. As no data was available, the conductivity in these calculations was assumed to be identical in the perpendicular and longitudinal directions. The thermal conductivity of the VIP core was calculated so the total thermal conductivity of the three layers was identical to the declared upper value of 0.005 W/(mK) by the producer (Porextherm 2009). In addition to verify that the simulation programs were reliable for the tested structures, these simulations also represented a control of the measured values in the experiment, especially the wetness sensor measurements. Mainly Field 1 and Field 2 were simulated as they represented the highest risk of moisture problems.

### 2.7 Condensation Control Calculations

Additional calculations that investigated condensation risk at the VIPs in Field 1 and Field 2 were performed. The basis of the calculations was the standard for hygrothermal performance of building components EN ISO 13788 (2001), which describes a method for addressing a critical limit for surface condensation accounting for the parameters mean monthly external temperature and RH, and internal temperature and moisture excess for the respective building. Instead of calculating the critical limit for condensation at one definite climate and internal moisture excess, the method was adapted to calculate the limit where condensation started for different internal moisture excess and external temperatures. That is, the external RH and the internal temperature were fixed at a probable value (80 % RH and 20°C). Moisture excess at the condensation limit was calculated for external temperatures from -40°C to 20°C. The calculations were performed for the gross structure, i.e. in the centre of the surface of a VIP. Thus, a surface resistance of 0.13 ($m^2K$)/W was used even if the standard EN ISO 13788 (2001) sets the worst-case surface resistance to 0.25 ($m^2K$)/W.

## 3 RESULTS AND DISCUSSION

### 3.1 U-value Calculations

The U-values of Field 1 and Field 3 calculated according to EN ISO 6946 (2007) are shown in Table 1. The U-value of F1 is calculated with a pristine VIP thermal conductivity of 0.005 W/(mK) (Porextherm 2009), with a common design conductivity of 0.008 W/(mK) accounting for VIP ageing, and with a conductivity for punctured VIPs of 0.020 W/(mK) (Binz et al. 2005). The linear thermal transmittance found for the VIP fastening bracket of tape-enveloped steel is used in the U-value calculations. Table 1 shows that 30 mm additional VIPs added to the reference field have a large influence on the U-value, even if the VIPs are punctured (F1 versus F3). The U-value of F1 with aged VIPs is at the level of today's requirements in Norway at 0.18 W/($m^2K$) (TEK 1997). F1 with pristine VIPs however, satisfies the requirements of the passive house standard in Norway NS 3700 (2010) (ageing of VIPs not accounted for). Investigations of VIP ageing may be found in Wegger et al. (2010).

The U-values of F2 and F4 are not shown here. That is, F4 is assumed to have about the same U-value as F1. However, some thermal bridges, like the thermal bridge between two floors, will not be insulated when the VIP retrofitting is performed at the inside. Insulation of thermal bridges represents a large advantage of adding insulation on the outside instead of the inside of a building. From a thermal insulation point of view, F1 is the best of the three alternatives evaluated. The potential moisture problems associated with this retrofitting method for improving the thermal performance of a wall are addressed in the following chapters.

**Table 1. U-values of Field 1 with different VIP properties, and the U-value of the reference field (F3).**

| Field | U-value ($W/(m^2K)$) |
|---|---|
| F1, pristine 30 mm VIPs* | 0.143 |
| F1, aged 30 mm VIPs | 0.181 |
| F1, punctured 30 mm VIPs | 0.262 |
| F3, reference field | 0.411 |
| Passive house requirement in Norway (NS 3700, 2010) | 0.15 |

*The small thermal bridge of the vertical VIP joints is not accounted for in the calculations. However, the conductivity of the VIPs is given a conservative value of 0.005 W/(mK) (< 0.005 W/(mK) Porextherm 2009).

## 3.2 Experimental Moisture and Condensation Results

The experimental moisture and condensation results are depicted as RH equivalent versus time at different locations inside selected test fields in Figs.8-11 (WB denotes wind barrier), between climate step 1 and 2 (from 30 to 40 % RH), climate step 2 and 3 (from 40 to 50 % RH) and climate step 3 and 4 (from 50 to 60 % RH). Figure 12 shows the measured temperatures in the reference field (F3).

None of the fields experienced condensation during climate step 1 or 2, with a RH of ~ 30 % and ~ 40 %, respectively. Hence, day 1 to day 15 of the experiment are only plotted for F2, thus depicting a case with no condensation as seen in Fig.8. The large alternation of RH in the climate room, up to 25 percentage points from the lowest to the highest value, can be seen in Fig.8. However, this problem was reduced after test day 15, when a different humidifier was installed.

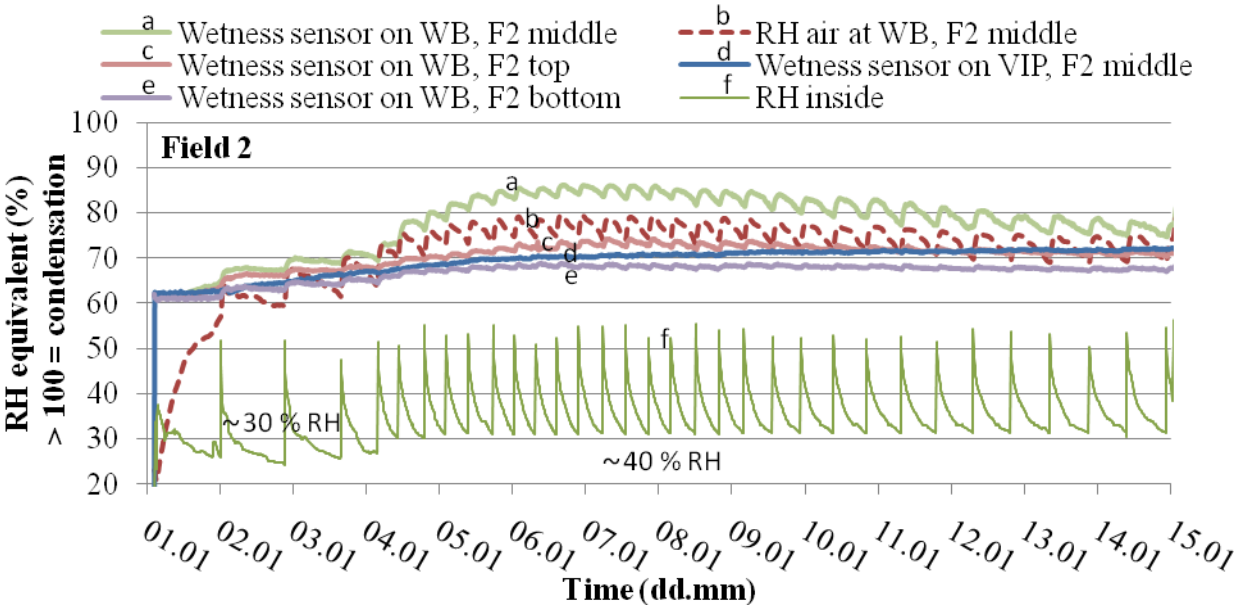


**Figure 8. Moisture sensors in F2 during climate step 1 and 2. The RH equivalent values of the four wetness sensors, as well as the RH air sensor, are shown. The climate room RH was ~ 30 % from day 1 to 4, and ~ 40 % from day 4 to 15 (graph f).**

Figure 9 shows F1, during the two climate steps with RH ~ 50 % and ~ 60 %. F1 experienced condensation at RH ~ 50 %, which was not expected for this climate step compared to numerical simulations, at least not after that short period of exposure. This might be caused by the relatively large alternations in RH at the inside climate room, seen in the lower graph (graph f) in Fig.9. The moisturising at the RH peak is possibly larger than the drying-out at the RH bottom. Small air leakages in the structure might also contribute to the measured condensation. The wetness sensor shows condensation (value above 100 %) when the RH air sensor shows about 95 % RH. A possible explanation is that the RH air sensor is located about 5 mm from the wind barrier. Moreover, the wetness sensor is more influenced by condensed water on the vapour barrier than the RH air sensor. The wetness sensor located on the joint between two VIPs shows lower values than the wetness sensor on the wind barrier. Assuming that both sensors have the same temperature, condensation may be caused by the small vapour resistance of the wind barrier. The wetness sensor on the VIP (behind the wind barrier) then becomes moisturised by the wet wind barrier, which causes the sudden increase at the wetness sensor on the VIP. Another influencing factor is convection over the joint between two VIPs (about 2 mm opening) that might dry the sensor somewhat. A third aspect may be time delay due to the small vapour resistance of the wind barrier, but this should not result in such a sudden increase. The wetness sensors at the top and the bottom have different development at the end of climate step 3. A possible explanation might be that the wetness sensor at the top experienced a lower RH caused by an (erroneous) increase in the outdoor temperature during the experiment (Fig.12). The increase at the wetness sensor at the bottom may be condensed water that runs down from the middle of the vapour barrier and moisturises the sensor.

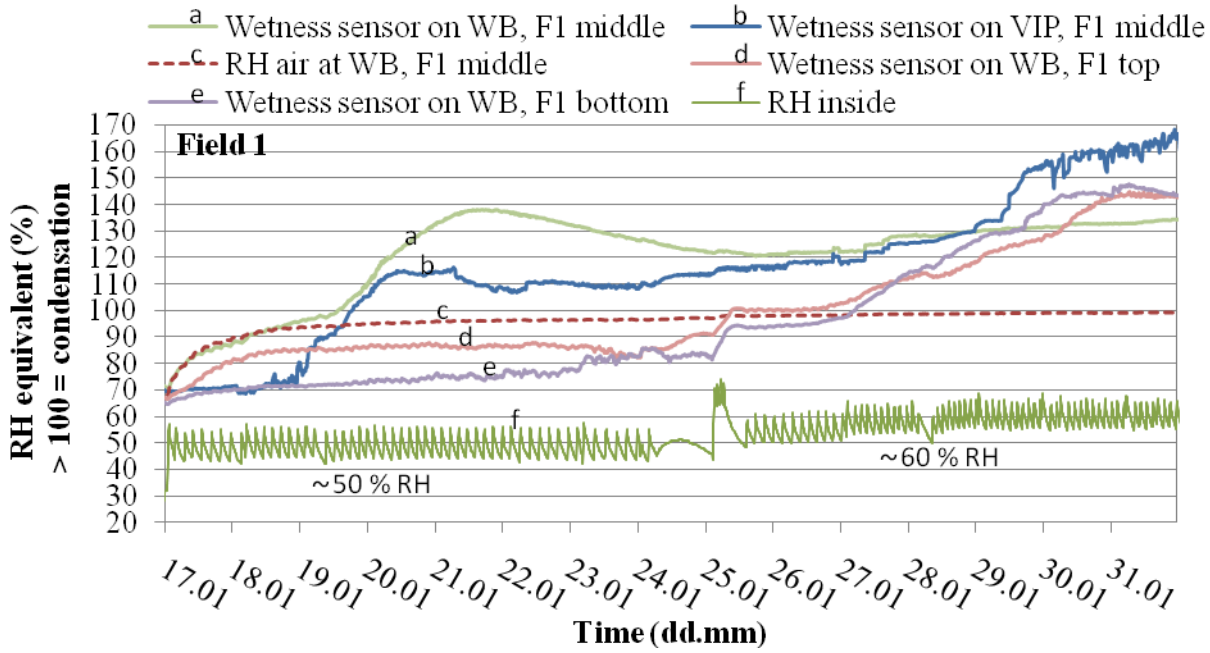


**Figure 9. Moisture sensors in F1 during climate step 3 and 4. The RH equivalent values of the four wetness sensors, as well as the RH air sensor are shown. The climate room RH was ~ 50 % from day 17 to 24, and ~ 60 % from day 26 to 32 (graph f).**

Figure 10 shows F2, during the two climate steps with RH ~ 50 % and ~ 60 %. In accordance with numerical simulations, the field experienced condensation during both climate step 3 and climate step 4. However, an interesting difference between F1 and F2 is the wetness sensors located on the VIPs. In F1 this sensor measured condensation at both climate steps, whereas in F2 this sensor measured condensation only for climate step 4 even if this field is less insulated (only 20 mm VIP). The temperatures measured at the warm side of the wind barrier

(Fig.12) depict that the wetness sensor at F1 had a higher temperature than the wetness sensor in F2, i.e. as expected, thus the reason why the wetness sensor at the joint between two VIPs in F2 did not show condensation is unclear. It might be caused by difference in workmanship of the wall or installation of the sensor. The somewhat rigid wind barrier was hard to fit properly and this might have caused air cavities between the VIP and the wind barrier that was different from F1 to F2. Another unexpected occurrence was the sudden drop at the wetness sensor at the joint between two VIPs (graph c) in Fig.10, which might be caused by a loosening of the sensor from the surface of the VIPs (however, this is not known).

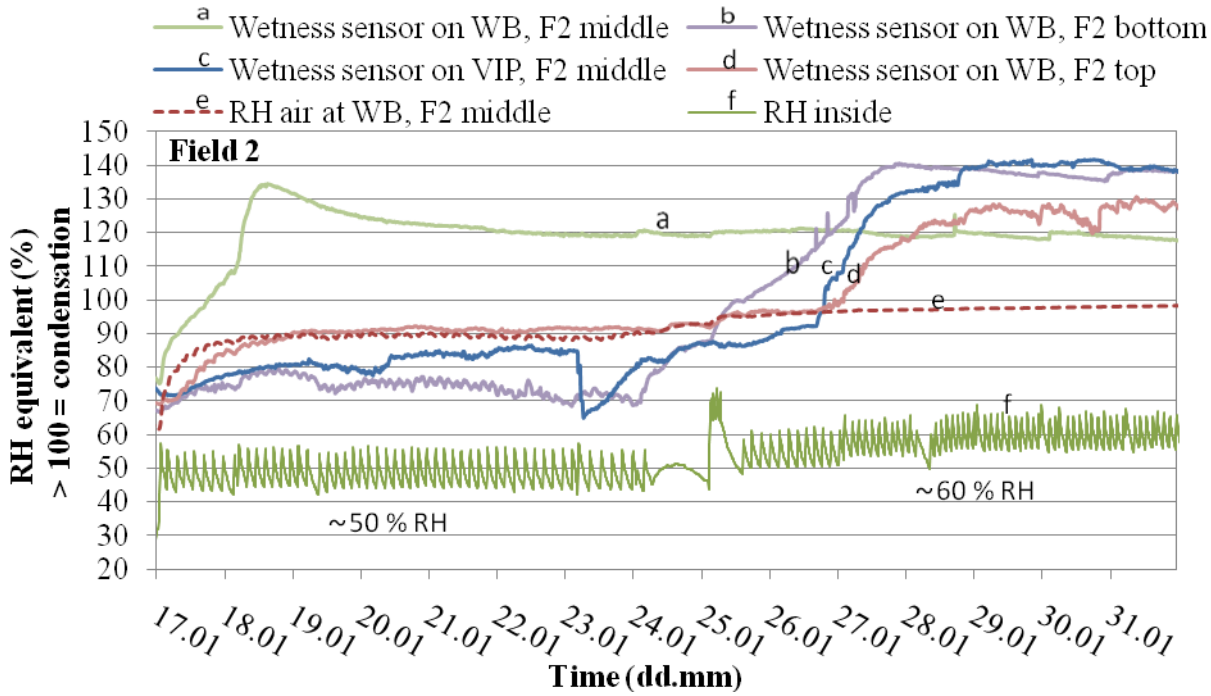


**Figure 10. Moisture sensors in F2 during climate step 3 and 4. The RH equivalent values of the four wetness sensors, as well as the RH air sensor, are shown. The climate room RH was ~ 50 % from day 17 to 24, and ~ 60 % from day 26 to 32 (graph f).**

Both Fig.9 and Fig.10 show a peak at the wetness sensors during condensation. The cause of these peaks might be the different sorption curves for spruce and paper, i.e. that the measured electrical resistance is in a sensitive area of the curve that describes the electrical resistance as a function of moisture content for spruce (as the moisture meter is calibrated with respect to spruce). A small decrease in RH might then give a large effect on the output value of the moisture meter. The graphical plots from F1 and F2 show a lower RH at the top and the bottom than in the middle of the fields. The high RH at the middle is due to the thermal bridge of the joint between two VIPs. The temperature at the structures laying above and below the module influences the temperature, and hence the RH at the top and the bottom. However, the surrounding structures cool down the module, therefore this only have a conservative effect, i.e. lower temperatures increase the RH. It is therefore clear that the thermal bridge at the joint between two VIPs is a critical point for condensation in the wall, together with the surfaces of the fastening brackets.

Field 4 with interior VIP retrofitting performed well during the entire test, i.e. no condensation occurred. RH at the middle of the wind barrier was about 50 % during the whole experiment, thus far from the risk of condensation. The results from F4 are thus in this context not found necessary to depict in graphical plots.

Figure 11 shows the reference field (F3) during climate step 3 and climate step 4. None of the sensors show condensation. The wetness sensors are not calibrated for temperatures below

0°C and are thus less trustworthy in F3. It is reasonable that the electrical resistance increases when the temperature drops below 0°C and the water freezes. Therefore, the values from the wetness sensors in F3 are lower than the RH air sensor. Condensation might be present in F3 without being measured. The time frame of the test is not necessarily long enough to give condensation, as F3 will experience a certain exsiccation to the outside climate room. The outside temperature was in addition increasing somewhat from the start of the climate step to the end as the cooling unit was manually de-iced for each climate step (Fig.12). This contributed to hold the RH air sensor on the wind barrier stable, as seen in Fig.11.

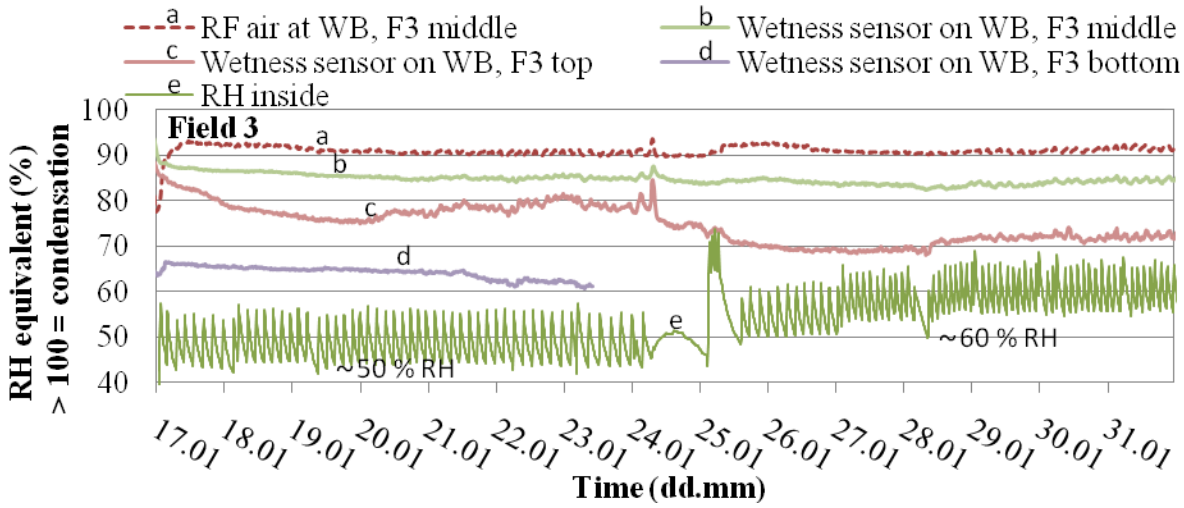


**Figure 11. Moisture sensors in F3 during climate step 3 and 4. The RH equivalent values of the three wetness sensors, as well as the RH air sensor, are shown. The wetness sensor at the bottom (graph d) stopped giving reliable outputs. The climate room RH was ~ 50 % from day 17 to 24, and ~ 60 % from day 26 to 32 (graph e).**

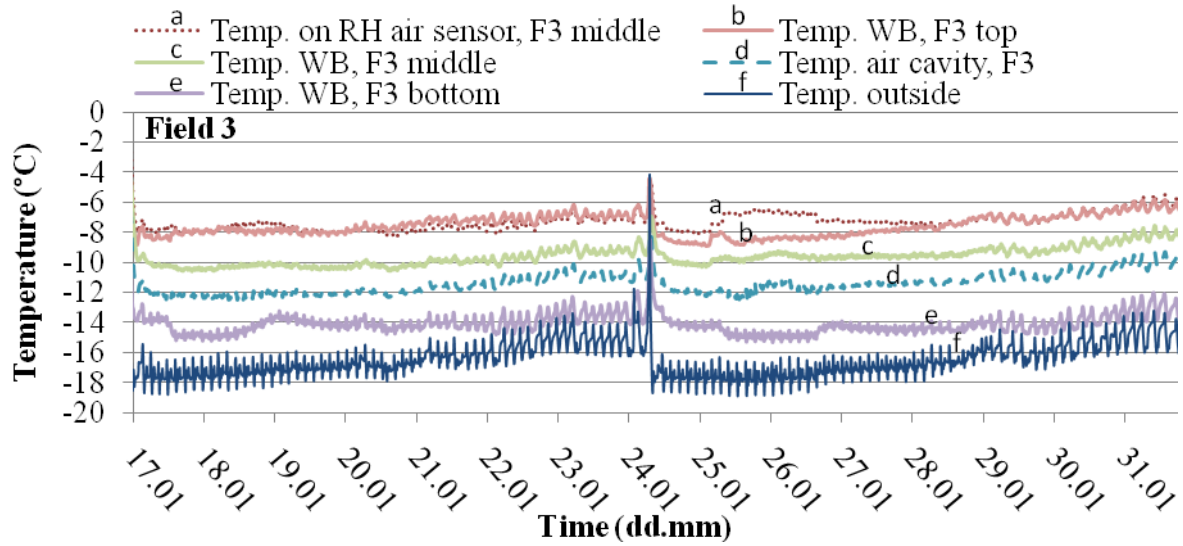


**Figure 12. Temperatures in F3 (reference) measured at the warm side of the wind barrier (WB) over the same time span and at the same locations as the wetness sensors shown in Fig.11. In addition, the temperature on the RH air sensor, the temperature in the air cavity on the inside of the wooden cladding, and the outside temperature in the climate room, are given.**

The results from the experiments allow for use of 30 mm VIPs at the outside of a 100 mm mineral wool wall to improve thermal insulation. However, the method of improving thermal insulation provide certain limitations to the interior and exterior climate. That is, not more severe than 20°C and an internal moisture excess of maximum 6 g/m$^3$ at the interior side, and -18°C and RH 60 % at exterior side. It must be emphasized that these results are only valid for VIPs in a pristine condition and when designing a real building the aged condition of the VIPs must be taken into account.

### 3.3 Comparison of Measured and Simulated Results

The WUFI simulation results and measured values from the wetness sensors and the RH air sensors are shown in Figs.13-15. These graphical plots show only the RH equivalent part of the wetness sensors, i.e. values above 100 are plotted as 100 % RH.

Figure 13 shows the WUFI and the wetness sensors results at the top of F2. The difference in RH values between the 1D and 2D simulation seems to be systematic and is probably caused by a lower temperature in the 2D simulation as depicted in Fig.14, which may be caused by the thermal bridge in the 2D simulation. The difference in wetness sensor measurements and simulated RH values seems mainly to be caused by the temperature difference as well. In Fig.14 the logged temperature graph is about 2.5°C warmer than the simulated values, which corresponds to a decrease in RH of about 20 percentage points at this temperature level. The low temperatures in the simulations may be caused by the application of the VIP upper limit declared thermal conductivity of 0.005 W/(mK) (Porextherm 2009), as the real thermal conductivity may be as low as 0.004 W/(mK) (Binz et al. 2005). Measurements have shown that both the conductivity and the thickness of different VIPs may vary, e.g. Grynning et al. (2010) measured conductivities somewhat higher than the declared ones and panel thicknesses that were less than stated.

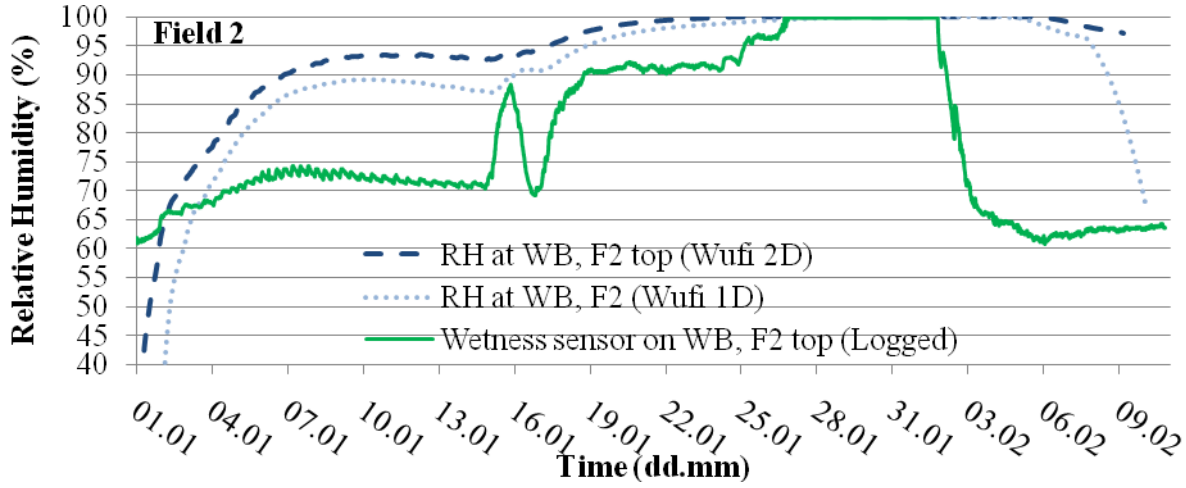


**Figure 13. Relative humidity simulated in WUFI 1D and WUFI 2D, and measured RH at top of F2.**

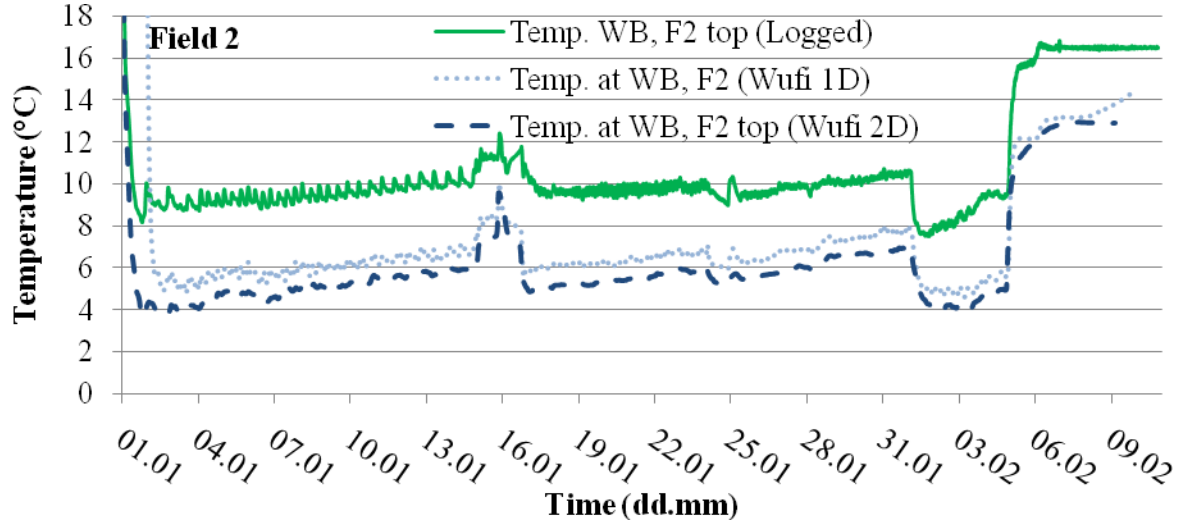


**Figure 14. Temperature simulated in WUFI 1D and WUFI 2D, and measured temperature at top of F2.**

Analogous plots (not presented here) as Fig.13 and Fig.14 were also made for F1, i.e. simulated and measured values of RH and temperature at the top of F1. The WUFI 1D and WUFI 2D simulation results compared well. However, the graph of the wetness sensor at the top showed also in this plot about 10 percentage points lower RH, except for the case of condensation. The difference seemed also here to be caused by a warmer temperature in the experimental results.

Figure 15 shows measured and simulated RH values at the middle of F1, where both the simulated and measured values compared quite well. The wetness sensor showed condensation when the two other graphs showed a RH of about 95 %, indicating that the wetness sensor represents a better condensation sensor than the regular RH air sensor due to the ability to register wetness on a surface. The small differences might be due to the eccentric location of the two other measurements, i.e. they are placed on a slightly warmer isotherm.

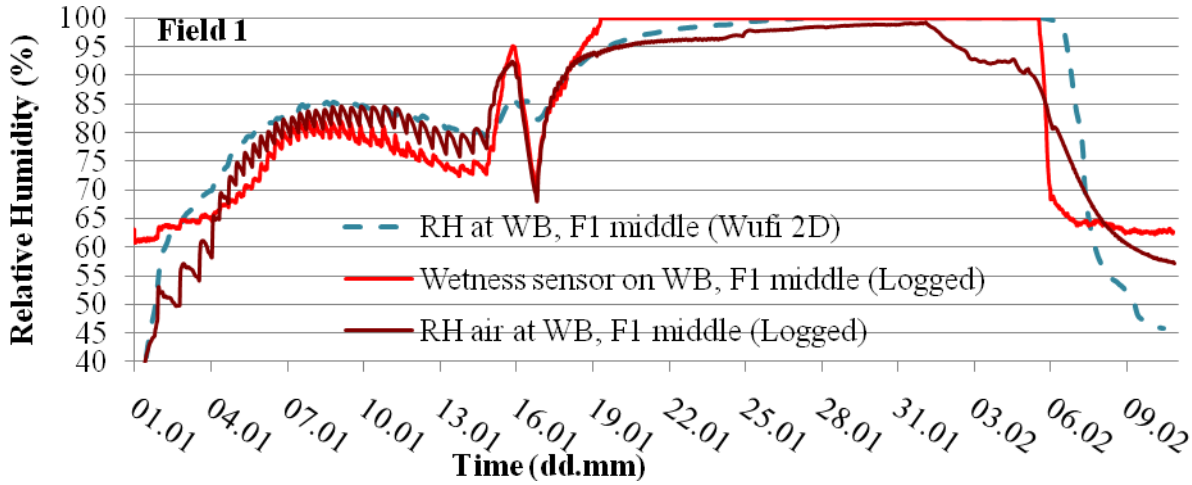


**Figure 15. RH simulated in WUFI 2D, and measured RH in the middle of F1.**

The effect of the drying-out process at the joint between two VIPs was questioned prior to the experiments. This mechanism is not numerically simulated, but the results have shown that the reduced temperature at this location has a larger influence on the RH than the drying-out effect, i.e. the RH at the joint between two VIPs was higher than in the centre of a VIP (sensors at middle compared to sensors at top). Generally, there is good agreement between the measured and simulated results. The differences registered seem mainly to be caused by inaccurate material properties applied in the simulations. These results show that both the WUFI simulations and the experimental results are reliable, and strengthen the reliability of the wetness sensor as a RH indicator.

### 3.4 Condensation Control

The calculations of condensation-start-limits are shown in Fig.16, illustrating what external temperature and internal moisture excess may cause condensation on the VIP surface for different conditions (thermal conductivities) of the VIPs. The calculations are based on an interior temperature of 20°C and an exterior RH of 80 % (except the upper graph with an exterior RH of 60 %). As for the U-value calculations, the thermal conductivities applied for pristine, aged and punctured VIPs are employed. It is important to emphasize that the tested constructions do not have a vapour barrier on the inside, and is hence considered as a worst-case wall compared to a more typical wall with a vapour barrier. The water vapour diffusion resistance of the materials at the interior of the VIPs is neglected, which represents a conservative simplification. It should also be noted that the risk of mould growth on wood in structures normally is assumed to start at a RH of 80 %.

Figure 16 shows that for an exterior RH level of 60 % and an exterior temperature of -18°C, the moisture excess must be 7.1 g/m$^3$ for condensation to occur at the VIPs in F1. This is equivalent with an indoor RH of 46 % at these conditions. During the experiment, condensation was not observed on the top or bottom of the fields before the inside RH was 60 %. Neglecting the water vapour diffusion resistance of the materials on the interior side of the VIPs may explain this difference. The material thermal conductivity might also deviate from the real value and cause an incorrect temperature factor. Lower thermal resistance at the surface due to air circulation in the climate rooms may also contribute to this difference. Furthermore, the calculations assume steady-state conditions, whereas the experiment was not run for a sufficient long time to reach complete steady-state.

The exterior temperature is to be the minimum mean temperature over three days in condensation calculations (SINTEF 471.111, 1999), and in design evaluations the aged value of the thermal conductivity of VIPs should be applied. Applying this for Oslo, Norway, with a mean minimum temperature over three days of -19.8°C (SINTEF 451.021, 2009), would give a maximum internal moisture excess of 4.7 g/m$^3$ (assuming an internal temperature of 20°C or higher). Note that the external RH at such low temperatures does not make a large difference to the calculations. Field 1 performs badly both thermally and hygrothermally if the VIPs are punctured.

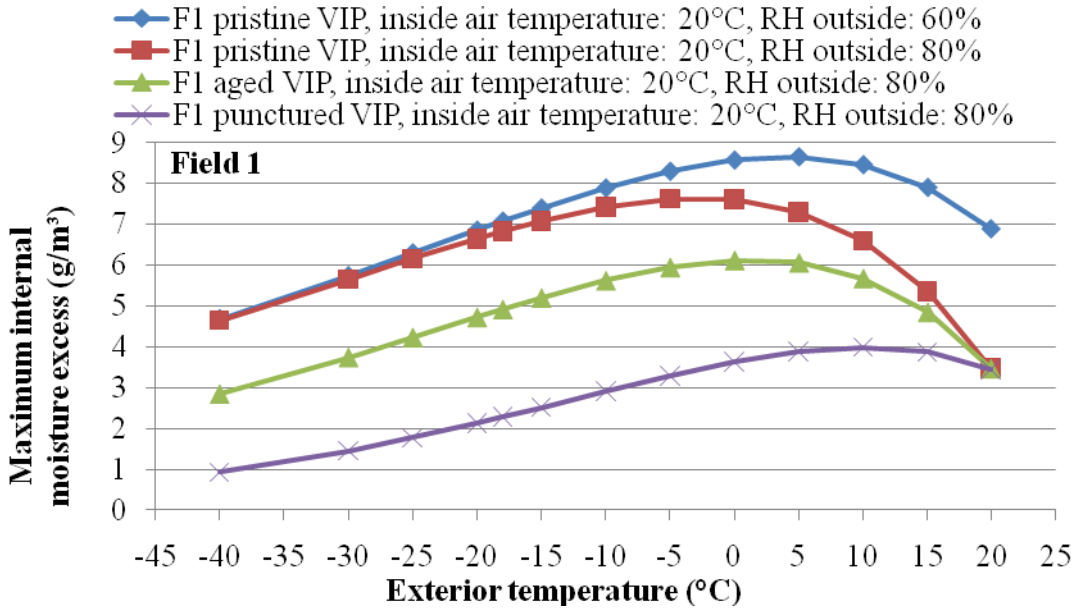


**Figure 16. Maximum moisture excess before condensation on VIP in F1.**

Similar graphical plots showing the condensation limits for F2 can be drawn (not depicted here). F2 is less insulated than F1 and thus cannot handle that large moisture excess before condensation occurs on the VIPs (compared to F1 in Fig.16 these graphs for F2 will be roughly shifted 1 g/m$^3$ lower). F2 might still perform well enough at many locations given a low moisture excess or a temperature within a specific range. Installing a ventilation system that prevents high indoor RH at wintertime, may also be a way of avoiding condensation in the wall.

These calculations only apply for the gross structure (i.e. at the centre of a VIP surface) and the temperature factor will be lower at the thermal bridges in the structure. However, this is normally only at small areas. A tight vapour barrier at the inside will avoid the condensation problem. Still, it is important to address these potential condensation problems without a vapour barrier as many are sceptical to adding a vapour tight material at the exterior side of an

insulated structure. A non-tight vapour barrier may lead to accumulation of moisture between two vapour tight materials. An increase in outdoor RH makes little difference at low exterior temperatures, but large difference when the exterior temperature is approaching the interior temperature. However, in Norway the relevance of the calculations is less for exterior temperatures above about 10°C, since the exterior RH is less likely to be as high as 80 % the higher the temperature is. In addition, the residents of a building start to ventilate way more at warm exterior temperatures, e.g. opening windows, etc., and hence, the air change rate increases and consequently the moisture excess is lowered. Furthermore, it should be noted that if a lower interior temperature (here < 20°C) had been used, the accepted moisture excess would be reduced.

# 4 CONCLUSIONS

Experimental work has been carried out on a test module built between two climate rooms with an indoor and an outdoor climate, respectively. The module consists of four fields, one reference field representing a timber frame wall built according to building regulations from the 1970s in Norway, and three fields representing different ways of improving the thermal insulation of the reference field by retrofitting with vacuum insulation panels (VIPs). Two of the fields were built with VIPs on the exterior side of the timber frame wall, one field with 20 mm VIPs and one field with 30 mm VIPs. The fourth field was built with VIPs retrofitted on the interior side. Temperature, relative humidity (RH) and surface wetness were measured during the experiment, as vapour tight VIPs on the exterior side may introduce condensation in a wall. In addition, numerical simulations for some of the experimental fields were performed. The simulations showed good correlation with the experiments. Calculations of threshold limits for condensation on the VIPs in the structure were performed with respect to different outdoor temperatures and internal moisture excess.

A tailor-made fastening bracket for VIPs was applied in the retrofitting experiments. The VIP fastening bracket reduced the thermal bridge of the joint between two VIPs compared with regular methods of fastening VIPs, i.e. using furring strips. Furthermore, a tailor-made moisture or wetness sensor was fabricated and applied in the experiments, which enabled moisture and condensation measurements directly on various surfaces. The wetness sensor proved to be relatively reliable for RH levels between 70 – 100 % and for indicating condensation. However, the sensor does not perform at temperatures below the freezing point, at RH levels below 60 %, or for repeating cycles of high and low RH. The results from the numerical simulations strengthened the reliability of the wetness sensor.

In total, the results from the experiment, the simulations, and the condensation controls conclude that timber frame buildings thermally insulated with 100 mm mineral wool, might be retrofitted at the exterior side by adding 30 mm VIPs in a continuous layer. Certain limits to outdoor temperature, internal moisture excess and indoor temperature are provided. The condensation calculations emphasized the importance of avoiding puncturing of VIPs and in addition to account for the aged conditions of VIPs. Hence, it is strongly emphasized that any potential or likely changes in the VIP thermal conductivity have to be accounted for during the design of retrofitting projects, where VIPs are applied on the exterior side of a wall.

# ACKNOWLEDGEMENTS

This work has been supported by the Research Council of Norway and several partners through the SINTEF and NTNU research project *"Robust Envelope Construction Details for*

*Buildings of the 21st Century*" (ROBUST) and "*The Research Centre on Zero Emission Buildings*" (ZEB). Franco Bløchlinger from Metallplan and the manufacturer Porextherm are acknowledged for supplying the vacuum insulation panel test samples. Ole Aunrønning (NTNU) and Egil Rognvik (SINTEF) provided valuable help during various experimental tasks.

## REFERENCES

R. Baetens, B. P. Jelle, J. V. Thue, M. J. Tenpierik, S. Grynning, S. Uvsløkk and A. Gustavsen, "Vacuum insulation panels for building applications: A review and beyond", *Energy and Buildings*, **42**, 147-172, 2010.

A. Binz, A. Moosmann, G. Steinke, U. Schonhardt, F. Fregnan, H. Simmler, S. Brunner, K. Ghazi, R. Bundi, U. Heinemann, H. Schwab, J. M. Cauberg, M. J. Tenpierik, G. Johannesson, T. Thorsell, M Erb and B. Nussbaumer, "Vacuum insulation in the building sector. Systems and applications (Subtask B)", Final report for the IEA/ECBCS Annex 39 HiPTI-project, 2005.

Building regulations, "Kap. 54 –Varmeisolering og tetthet" (Norwegian building regulations of 1969, chapter 54 –Thermal insulation and air tightness), 1969.

EN ISO 6946, "Building components and building elements - Thermal resistance and thermal transmittance - Calculation method", 2007.

EN ISO 10211, "Thermal bridges in building construction - Heat flows and surface temperatures - Detailed calculations", 2007.

EN ISO 10456, "Building materials and products - Hygrothermal properties - Tabulated design values and procedures for determining declared and design thermal values", 2007.

EN ISO 13788, "Hygrothermal performance of building components and building elements - Internal surface temperature to avoid critical surface humidity and interstitial condensation - Calculation methods", 2001.

S. Grynning, B. P. Jelle, S. Uvsløkk, A. Gustavsen, R. Baetens, R. Caps and V. Meløysund, "Hot Box Investigations and Theoretical Assessments of Miscellaneous Vacuum Insulation Panel Configurations in Building Envelopes", Accepted for publication in *Journal of Building Physics*, 2010.

J. Kneifel, "Life-cycle carbon and cost analysis of energy efficiency measures in new commercial buildings", *Energy and buildings*, **42**, 333-340, 2010.

McKinsey, "Pathways to a low-carbon economy", Version 2 of Global Greenhouse Gas Abatement Cost Curve, McKinsey & Company, 2009.

NS 3700, "Kriterier for passivhus og lavenergihus. Boligbygninger"(Criteria for passive houses and low energy houses. Residential buildings), 2010.

Porextherm, 2009, "Vacupor NT – B2, data sheet", http://www.porextherm.com/web/pdfdownload.htm?ID=255&doctype=PDF_EN&lang=en&externeswindow=2&ts=1270722658, Retrieved 08.04.2010, 2009.

SINTEF 451.021, SINTEF Building Research Design Guides no. 451.021, ”Klimadata for termisk dimensjonering og frostsikring” (Climate data for thermal design and frost control), SINTEF Building and Infrastructure, Norway, 2009.

SINTEF 471.111, SINTEF Building Research Design Guides no. 471.111, ”Beregningsmetode for å unngå kondens eller muggvekst på overflater” (Calculation method for avoiding condensation or mould growth at surfaces), SINTEF Building and Infrastructure, Norway, 1999.

SINTEF 523.002, SINTEF Building Research Design Guides no. 523.002, ”Yttervegger over terreng. Egenskaper og konstruksjonsprinsipper. Krav og anbefalinger” (Building walls above ground. Properties and construction principles. Requirements and recommendations), SINTEF Building and Infrastructure, Norway, 2008.

Statistics Norway, ”Boliger, etter bygningstype og byggeår (K)” (Buildings, ranged by building type and construction year), Table 06266, 2009.

TEK, §8-2, Energibruk (energikrav revidert i 2007) (Building regulations of 1997, energy demands corrected in 2007, §8-2, Energy), 1997.

M. J. Tenpierik and H. Cauberg, ”Analytical models for calculating thermal bridge effects caused by thin high barrier envelopes around vacuum insulation panels”, *Journal of Building Physics*, **30,** 185-215, 2007.

M. Tenpierik, ”Vacuum insulation panels applied in building constructions”, *Ph.D. thesis*, Technische Universiteit Delft, Netherlands, 2009.

THERM Finite Element Simulator, version 5.2.14, 2003.

E. Wegger, B. P. Jelle, E. Sveipe, S. Grynning, A. Gustavsen, R. Baetens and J. V. Thue, ”Ageing effects on thermal properties and service life of vacuum insulation panels”, Submitted for publication in *Journal of Building Physics*, 2010.

M. K. Willems, K. Schild and G. Hellinger, ”Numerical investigation on thermal bridge effects in vacuum insulating elements”, *Proceedings of 7th International Vacuum Insulation Symposium*, EMPA, p. 145–152, 2005.

WUFI 1D pro, version 4.2 NBI/NTNU, Release 4.2.0.421.DB.24.63, 2008.

WUFI 2D, version 3.3, Release 3.3.1.60.DB.24.63, 2010.